Eur. Phys. J. Appl. Phys. (2012) 59: 10403
DOI: 10.1051/epjap/2012110476

THE EUROPEAN PHYSICAL JOURNAL
APPLIED PHYSICS

Regular Article

An efficient continuum model for CNTs-based bio-sensors

P. Soltani[1,a], O. Pashaei Narenjbon[1], M.M. Taherian[3], and A. Farshidianfar[2]

[1] Department of Mechanical Engineering, Semnan Branch, Islamic Azad University, Semnan, Iran
[2] Department of Mechanical Engineering, Ferdowsi University of Mashhad, Mashhad, Iran
[3] Young Researchers Club, Semnan Branch, Islamic Azad University, Semnan, Iran

Received: 18 December 2011 / Received in final form: 11 May 2012 / Accepted: 25 May 2012
Published online: 16 July 2012 –

Abstract. The present paper proposes a new equation utilizing the nonlocal Euler-Bernoulli beam model to investigate the linear transverse vibration of an embedded single-walled carbon nanotube (SWCNT) which incorporates an extra-added nanoparticle. The elastic behavior of the surrounding medium is simulated by the Pasternak-type foundation model. Hamilton's principle is applied to derive the governing equation, and the natural frequencies are obtained by the Galerkin method. The numerical results are compared with the molecular dynamics (MD) simulation as well as with the local continuum approach in the previous literature, to validate the nonlocal continuum elastic model. Unlike the classical continuum model, the present new approach shows acceptable accuracy and good agreement to the MD approximation. The results indicate that the fundamental frequencies are significantly dependent on the attached mass and boundary conditions. To study the effects of supported end conditions, three typical boundary conditions, namely clamped-clamped, clamped-pinned and pinned-pinned, are simulated. It is found that an attached mass causes a noticeable reduction in natural frequencies, in particular, for the clamped-clamped boundary condition, a stiff medium, stocky SWCNT and a small nonlocal parameter. In addition, when the position of the added nanoparticle is closer to the middle point of SWCNT length, the mass sensitivity is increased. Detailed results demonstrate that the present equation-based nonlocal continuum theory can be utilized for SWCNT-based mass sensor, efficiently.

1 Introduction

Since carbon nanotubes (CNTs) demonstrate exceptional and superior mechanical, chemical, electrical and thermal properties [1–5], they have many new applications in nanomechanical and nanoelectromechanical systems (NEMS) such as nanosensors [6,7], nano-actuators [8,9] and electrochemical sensing systems [10–12].

CNTs play significant roles in the biological applications [13–15], especially in bio-sensing [16], and there have been several attempts to adapt CNTs as ultrasensitive nano-bio sensors [9,17]. CNT-based nano-bio sensors have been driven by the experimental evidence and the development of nano-bio sensors and nanoscale bioreactor systems based on CNTs are experimentally investigated to show that biological entities such as proteins, enzymes and bacteria can be immobilized either in the hollow cavity or on the surface of carbon nanotubes [18].

Recently, mass detection based on mechanical resonators has been the subject of growing research interest. The advances in lithography and materials synthesis have permitted the fabrication of nanomechanical resonators, which have been performed as a more accurate mass sensor. The essence of mass sensing in a resonator is based on the fact that the vibration behavior of a resonator is sensitive to changing the total mass of the system, including the mass of the system and added particle. The change in the attached mass causes a change in the resonant frequency, and because the greater relative changes of mass, mechanical mass nanosensors with nanoscale dimensions are more sensitive to large molecules in comparison to the micro-sensors [19]. Consequently, the dynamical behavior of a CNT-based mass sensor has become important. Theories such as elastic continuum mechanics, as well as molecular dynamics (MD) simulations, are used for modeling vibration of behaviors of these systems, because they can accurately and cost-effectively produce results that closely approximate the real behavior of CNTs [20–23]. There is little research concerned with the vibration of CNTs with an attached mass using MD simulation. For instance, Georgantzinos and Anifantis [24] applied a spring-mass-based finite element method for investigating the vibrational behavior of single- and multi-walled carbon nanotubes (MWCNTs) with an added mass. The paper demonstrates that different geometric parameters such as the diameter and length of CNTs with cantilevered and bridged boundary conditions have significantly influenced the mass sensing behavior of CNTs. Further, they showed that SWCNTs are more sensitive

[a] e-mail: p.soltani@semnaniau.ac.ir

than MWCNTs. In another work, Arash et al. [25] focused on the detection of gas atoms by using the vibrational analysis of the SWCNTs as nanosensors. The MD simulation was developed to determine the shift frequency as well as to investigate the effects of gas atoms density on the SWCNTs, the size of SWCNTs and the type of boundary conditions on the sensitivity of nanomass sensors. However, the MD simulation involves complex computational processes, and is still formidable and expensive, especially for large-scale nanostructures and continuum elastic theories are widely utilized to simulate the vibration of CNTs as a mass detector instead. The potential of SWCNTs as a cantilevered and bridged mass sensor is explored using the classical Euler-Bernoulli beam theory by Chowdhury et al. [18]. The results show that the mass sensitivity of CNTs can reach up to 10^{-24} kg. Joshi et al. [26] investigated the resonant frequency of the fixed-free and bridged SWCNT with an attached mass in which the SWCNTs are depicted as thin shells with thickness using the finite element method (FEM). They examined how the sensitivity of CNTs increases with the increase of attached mass, especially for short SWCNTs. The effect of tip rigidity and added mass on the resonant frequency of a cantilever SWCNT has been studied by developing a local continuum bending model [27]. Since the classical or local elasticity theory in the above-mentioned studies is not size dependent, the nonlocal elastic theory is utilized to consider the small-scale effect in the dynamical model of the mass sensors. Murmu and Adhikari [28] examined the longitudinal vibration of SWCNTs when a buckyball is attached to them based on the nonlocal Euler-Bernoulli model. The results have shown that the change in resonant frequency due to the added mass and the nonlocal parameter could be important on the mechanical behavior of nanoresonators. They also proposed the nonlocal elasticity theory to investigate the vibrational behavior of CNTs-based cantilever mass sensors with two practical configurations of attached mass, namely, point mass and distributed mass [29]. The detailed results have shown that the nature of added mass should be efficiently considered as the distributed mass. A nonlocal elastic rod model is developed to study the axial vibrations of SWCNTs as a mass sensor by Aydogdu and his co-worker Filiz [30]. The effects of differing length, attached mass, boundary conditions and nonlocality on the natural frequency have been shown.

According to the best of our knowledge, no research has investigated the suitability of the nonlocal elasticity theory for simulating the transverse vibration of the SWCNT as a mass sensor device. In other words, the nonlocal continuum model may move away obviously from the MD approximation or experimental methods. In this paper, a nonlocal Euler-Bernoulli model is used to analyze the free transverse vibration of an embedded SWCNT with an attached nanoparticle. The equation of motion is derived by Hamilton's principle and solved by the Galerkin method. For the first time, the nonlocal Euler-Bernoulli theory is compared with a MD simulation and the local continuum approach. Therefore, a certain condition is determined in which the results of the continuum model agree well with the atomistic-based study with a reasonable accuracy. Moreover, the Pasternak-type foundation is applied with three typical boundary conditions to demonstrate the mechanical behavior of the nanosensor more naturally. Finally, the shift of frequency is discussed for various parameters such as stiffness of the model, aspect ratio, the nonlocal parameter and physical location of the attached mass.

2 Modeling

Figure 1 shows a clamped-clamped SWCNT with an attached mass m in location X_m that is modeled by the Euler-Bernoulli beam theory. E, ρ, A, L and d_o indicate Young's modulus, density, cross-section area, length and outer diameter of the SWCNT, respectively. The surrounding elastic medium is simulated as a Pasternak-type foundation that represents a generalized and realistic illustration of mechanical interaction between the SWCNT and its medium.

The transverse vibration is assumed in the x-z plane. Based on the Euler-Bernoulli beam theory, the displacement field at any point in the SWCNTs along the x- and z-axes, denoted by $u_x(x, z, t)$ and $u_z(x, z, t)$, respectively, as:

$$u_x(x, z, t) = u(x, t) - z\frac{\partial w(x, t)}{\partial x}, \quad u_z(x, z, t) = w(x, t), \tag{1}$$

where $u(x, t)$ and $w(x, t)$ are displacement functions in the mid-plane of the nanobeam for axial and transverse coordinates, in that order, and t is time. The linear and nonzero strain-displacement relations are given as:

$$\varepsilon_{xx} = \frac{\partial u}{\partial x} - z\frac{\partial^2 w}{\partial x^2}, \tag{2}$$

where ε_{xx} is the axial strain.

Hence, the first variation of the total strain energy U in the SWCNTs on the time interval $[0, T]$ can be calculated from:

$$\begin{aligned}\delta\int_0^T U\mathrm{d}t &= \int_0^T\int_0^L\int_A \sigma_{xx}\delta\varepsilon_{xx}\mathrm{d}A\mathrm{d}x\mathrm{d}t \\ &= \int_0^T\int_0^L\left[-\frac{\mathrm{d}N_x}{\mathrm{d}x}\delta u - \frac{\mathrm{d}^2M_x}{\mathrm{d}x^2}\delta w\right]\mathrm{d}x\mathrm{d}t \\ &\quad + \int_0^T\left[N_x\delta u + \frac{\mathrm{d}M_x}{\mathrm{d}x}\delta w - M_x\delta\frac{\mathrm{d}w}{\mathrm{d}x}\right]_{x=0}^{x=L}\mathrm{d}t,\end{aligned} \tag{3}$$

where σ_{xx} is the axial stress and δ is the variation operator. Moreover,

$$(N_x, M_x) = \int_A \sigma_x(1, z)\mathrm{d}A, \tag{4}$$

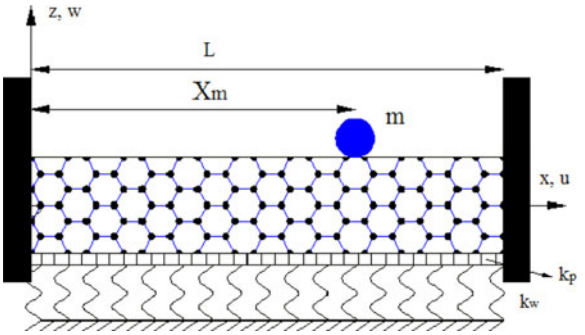

Fig. 1. (Color online) The SWCNT embedded in an elastic medium with an attached mass.

are the normal resultant force and bending moment, respectively.

The first variation of the kinetic energy K on the time interval $[0, T]$ for SWCNTs with the attached mass m in the X_m position can be written as follows:

$$\begin{aligned}\delta\int_0^T K\mathrm{d}t &= \int_0^T\int_0^L\int_A \rho\left(\frac{\partial u_x}{\partial t}\delta\frac{\partial u_x}{\partial t}+\frac{\partial u_z}{\partial t}\delta\frac{\partial u_z}{\partial t}\right)\mathrm{d}A\mathrm{d}x\mathrm{d}t\\ &\quad+\int_0^T\int_0^L m\Delta(x-X_m)\frac{\partial u_z}{\partial t}\delta\frac{\partial u_z}{\partial t}\mathrm{d}x\mathrm{d}t\\ &=\int_0^T\int_0^L\left[-I_0\frac{\partial^2 u}{\partial t^2}\delta u-(I_0+m\Delta(x-X_m))\right.\\ &\quad\left.\times\frac{\partial^2 w}{\partial t^2}\delta w\right]\mathrm{d}x\mathrm{d}t+\int_0^L\left[I_0\frac{\partial u}{\partial t}\delta u\right.\\ &\quad\left.+(I_0+m\Delta(x-X_m))\frac{\partial w}{\partial t}\delta w\right]_{t=0}^{t=T}\mathrm{d}x\end{aligned} \tag{5}$$

where $\Delta(\cdot)$ is the Dirac-delta function and $I_0=\int_A\rho\mathrm{d}A=\rho A$ is the mass per unit length of the SWCNT.

The relationship between displacement and transverse force of the Pasternak-type foundation is assumed to be $p=k_w w-k_p\frac{\partial^2 w}{\partial x^2}$, where k_w and k_p are the Winkler stiffness and the shearing layer stiffness of the foundation, respectively, and p is the force per unit length. Therefore, the first variation of the virtual work W done by external distributed load p on the time interval $[0, T]$ is obtained as:

$$\begin{aligned}\delta\int_0^T W\mathrm{d}t &= \int_0^T\int_0^L p\delta w\mathrm{d}x\mathrm{d}t\\ &=\int_0^T\int_0^L\left[k_w w-k_p\frac{\partial^2 w}{\partial x^2}\right]\delta w\mathrm{d}x\mathrm{d}t.\end{aligned} \tag{6}$$

The governing equations of motion of the SWCNTs can be derived by Hamilton's principle as:

$$\delta\int_0^T[K-(U-W)]\mathrm{d}t=0. \tag{7}$$

Substituting equations (3), (5) and (6) into equation (7) and setting the coefficient δw to zero lead to the differential equation of motion as:

$$\frac{\partial^2 M_x}{\partial x^2}+k_p\frac{\partial^2 w}{\partial x^2}-k_w w-\rho A\frac{\partial^2 w}{\partial t^2}-m\Delta(x-X_m)\frac{\partial^2 w}{\partial t^2}=0, \tag{8}$$

and the natural boundary conditions at the ends of the SWCNT are:

$$w=0 \text{ or } \frac{\partial M_x}{\partial x}=0,\ \frac{\partial w}{\partial x}=0 \text{ or } M_x=0, \qquad \text{at } x=0,\ L. \tag{9}$$

The one-dimensional stress constitutive relation of the nonlocal Euler-Bernoulli beam model becomes [31]:

$$\sigma_{xx}-(e_0a)^2\frac{\partial^2\sigma_{xx}}{\partial x^2}=E\varepsilon_{xx}. \tag{10}$$

In the above equation, e_0a represents a nonlocal parameter that reveals the nanoscale effect on the response of structures. In addition, e_0 and a are the material constant and an internal characteristic length, in that order [32]. Using equations (10), (2) and (4), the bending moment of SWCNTs in terms of displacement can be obtained as:

$$M_x-(e_0a)^2\frac{\partial^2 M_x}{\partial x^2}=-EI\frac{\partial^2 w}{\partial x^2}, \tag{11}$$

where $I=\int_A z^2\mathrm{d}A$ is the second moment of area. By inserting equation (11) into equation (8), the nonlocal transverse linear equation of motion for a embedded SWCNTs with an attached mass m is written as:

$$\begin{aligned}&-\rho A\frac{\partial^2 w}{\partial x^2}-k_w w+k_p\frac{\partial^2 w}{\partial x^2}-m\Delta(x-X_m)\frac{\partial^2 w}{\partial x^2}\\ &-EI\frac{\partial^4 w}{\partial x^4}+(e_0a)^2\left[m\Delta^{(2)}(x-X_m)\frac{\partial^2 w}{\partial t^2}\right.\\ &+2m\Delta^{(1)}(x-X_m)\frac{\partial^3 w}{\partial x\partial t^2}+m\Delta(x-X_m)\frac{\partial^4 w}{\partial x^2\partial t^2}\\ &\left.+\rho A\frac{\partial^4 w}{\partial x^2\partial t^2}+k_w\frac{\partial^2 w}{\partial x^2}-k_p\frac{\partial^4 w}{\partial x^4}\right]=0,\end{aligned} \tag{12}$$

where $\Delta^{(n)}(\cdot)$ is the nth derivative of the Dirac-delta function. It should be noted when the nonlocal e_0a, the Pasternak (k_w, k_p) parameters and the value of attached mass m are taken as zero in the above equation, the local equation of motion of an Euler-Bernoulli beam model is easily obtained [33].

The Galerkin method is used for solving equation (12). This method is an effective simple approach for various engineering problems and the associated boundary conditions to determine the linear free vibrational frequencies

of the nonlocal Euler-Bernoulli nanobeam model. In the modal form, the transverse dynamic displacement of the SWCNTs [33] is written as:

$$w(x,\,t) = \sum_{n=1}^{\infty} \phi_n(x) q_n(t), \tag{13}$$

where $q_n(t)$ is a time-dependent function and $\phi_n(x)$ is the natural mode shape of the nanotube. In this article, three standard boundary conditions are investigated for the SWCNT that are introduced as:

1. A simply supported beam or a beam with pinned-pinned (P-P) boundary condition at both ends:

$$\phi_n(x) = \sin\left(\frac{n\pi x}{L}\right). \tag{14}$$

2. A beam with clamped-pinned (C-P) boundary condition at both ends:

$$\begin{aligned}\phi_n(x) = [&\cos(\beta_n x) - \cosh(\beta_n x) \\ &-C\left(\sin(\beta_n x) - \sinh(\beta_n x)\right)],\end{aligned} \tag{15a}$$

in which

$$C = \frac{\cos(\beta_n L) - \cosh(\beta_n L)}{\sin(\beta_n L) - \sinh(\beta_n L)}, \tag{15b}$$

$$\beta_n = \frac{(2n+1)\,\pi}{4L}. \tag{15c}$$

3. A beam clamped at both ends or clamped-clamped (C-C) boundary condition:

$$\begin{aligned}\phi_n(x) = [&\cos(\beta_n x) - \cosh(\beta_n x) \\ &-C\left(\sin(\beta_n x) - \sinh(\beta_n x)\right)],\end{aligned} \tag{16a}$$

in which

$$C = \frac{\cos(\beta_n L) - \cosh(\beta_n L)}{\sin(\beta_n L) - \sinh(\beta_n L)}, \tag{16b}$$

$$\beta_n = \frac{(2n-1)\,\pi}{2L}. \tag{16c}$$

Applying equations (13)–(16) into equation (12) and multiplying both sides of the resulting equation with $\phi_m(x)$, then integrating it over the interval $[0,\ L]$ and considering the orthogonality condition and general properties of Dirac-delta function [31], the ordinary differential equation of the fundamental mode ($n = 1$) of the generalized deflection for three classical boundary conditions can be written as:

$$\frac{\mathrm{d}^2 q(t)}{\mathrm{d}t^2} + \left(\frac{K_{\mathrm{eq}}}{M_{\mathrm{eq}}}\right) q(t) = 0, \tag{17}$$

where K_{eq} and M_{eq} are the equivalent values of stiffness and mass of the vibrational system, respectively, that are described in detail in the Appendix. Therefore, the fundamental frequency f_n can be defined as follows:

$$f_n = \frac{1}{2\pi}\sqrt{\frac{K_{\mathrm{eq}}}{M_{\mathrm{eq}}}}. \tag{18}$$

3 Validation

This study provides a new equation based on the nonlocal Euler-Bernoulli beam theory to predict the mass sensing characteristics of a SWCNT-based mass sensor. In the previous study [18], Chowdhury et al. have modeled a SWCNT using the local continuum mechanics-based approach to detect the mass of biological objects. Hence, they approximated the following expression to obtain the resonant frequency f_n:

$$f_n = \frac{1}{2\pi}\sqrt{\frac{192EI/L^3}{\frac{13}{35}\rho AL + m}}. \tag{19}$$

As the size of SWCNTs is on the nanoscale, it is significant to regard the small-scale effect. This has raised a major challenge to the local continuum mechanics that assumes the stress at a reference point as a function of the strain state at that point in the material. Therefore, the local or classical continuum mechanic cannot predict accurately the behavior of nanoscale materials. Unlike the local theory, the nonlocal elasticity theory observes that the stress at a given point in a body depends not only on the strain at that point but also on at all points of the body [32]. Reference [18] utilized local elasticity and adapted a simplified method with approximate results. Therefore, this model may consequently produce significant errors in its results.

As mentioned before, the MD simulation has been used to study the transverse vibrational behavior of SWCNTs with C-C boundary condition when a nanoparticle is added at the midpoint, in a previous study [24]. Molecular dynamics methods simulate the exact geometry and mechanical behavior of the CNT, revealing the precise results of natural frequencies and mode shapes of vibration. To see the validity of the present method, the obtained results are compared with a MD study [24] in this literature.

First, in Figure 2, the fundamental frequencies that were obtained by MD approximation [24], local continuum approach (Eq. (19)) [18] and the present method are plotted against the mass ratio MR (m/m_r, where m_r is the mass of a carbon nucleus) for the different nonlocal parameters. The armchair (6, 6) SWCNT is used to plot this figure. The figure reveals that achieved results from the present technique agree well with the MD method in the nonlocal parameter of 1 nm $< e_0 a <$ 2 nm. In addition, it can be seen that local elasticity causes a significant deviation in the obtained frequency compared with the nonlocal model used in this paper. Furthermore, it can be seen that when the nonlocal parameter $e_0 a$ is set as zero in equation (12), the new present equation is more accurate than the previous investigation [18].

To represent the validity of the presented model more clearly, and as second check, the shift of the frequency parameter is presented in Figure 3 against the mass ratio MR for the three approaches that were mentioned above. The shift of frequency SF is defined as a parameter that indicates the changes of frequency for a SWCNT with no

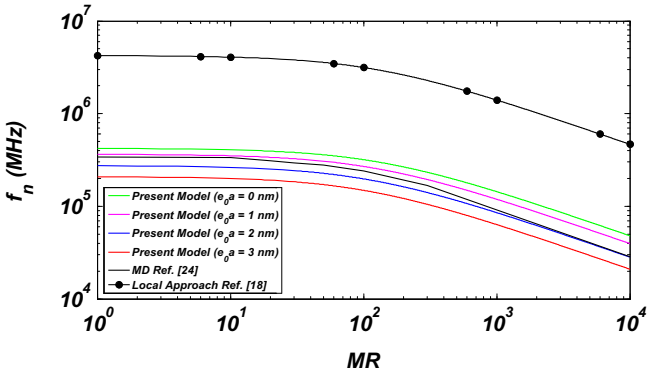

Fig. 2. (Color online) The fundamental frequency f_n against the mass ratio MR for a clamped-clamped supported (6, 6) SWCNT with 6 nm length.

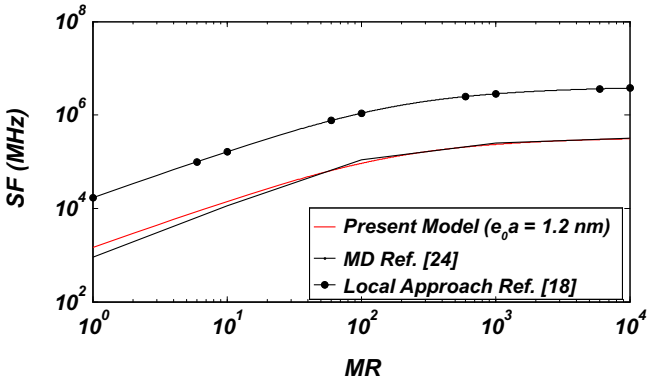

Fig. 3. (Color online) The shift of frequency SF against the mass ratio MR for a clamped-clamped supported (6, 6) SWCNT with 6 nm length.

added mass ($m = 0$) in comparison with a SWCNT containing attached mass ($m \neq 0$) as follows:

$$SF = f_n\big|_{(m=0)} - f_n\big|_{(m\neq 0)}. \tag{20}$$

In this specific situation ($e_0a = 1.2$ nm, that is in the range of 1 nm $< e_0a <$ 2 nm), detailed results indicate that the error between the nonlocal Euler-Bernoulli model and the MD simulation is insignificant.

According to Figures 2 and 3, the local mechanics approach shows an important deviation from the nonlocal model and also a MD simulation. Moreover, unlike the continuum elasticity theories, the MD simulation is computationally and cannot be used for a large system. Therefore, the nonlocal continuum mechanics approach could be efficiently employed to investigate the vibration of SWCNT including a nanoparticle.

4 Results and discussion

In the present study, the fundamental frequency equation f_n is obtained according to the nonlocal Euler-Bernoulli beam model for SWCNTs with three standard boundary conditions as a mass sensor. The mass of the attached nanoparticle can influence the resonant frequency effectively and is consequently considered here as a key parameter. The geometrical and mechanical properties are assumed to be a (16, 12) SWCNT [34]. Moreover, the constants of the Pasternak-type medium, nonlocal parameter and aspect ratio of SWCNTs are taken as: $k_w = 1$ Mpa, $k_p = 1$ nN, $e_0a = 2$ nm, $L/d_o = 25$ [20].

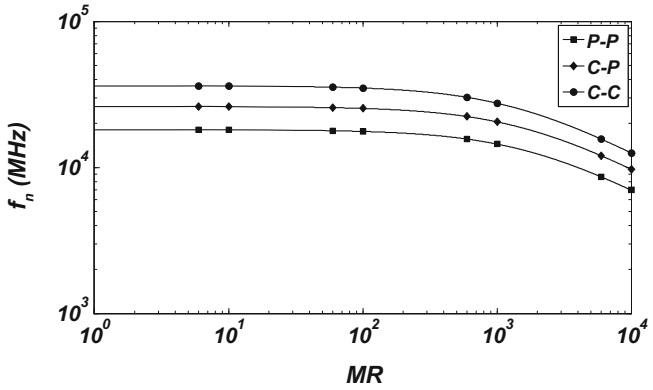

Fig. 4. The fundamental frequency f_n against the mass ratio MR for three standard boundary conditions.

In Figure 4, the fundamental frequency f_n of a SWCNT with a nanomass at the midpoint ($X_m/L = 1/2$) for three typical boundary conditions is given as a function of the mass ratio MR. Increasing the mass of the attached nanoparticle increases the total mass of the system M_{eq} and the fundamental frequency decreases as shown. This frequency reduction exaggerates for nanoparticles with larger MR. Also, the results show that the increasing the SWCNT stiffness due to the boundary conditions from P-P to C-C causes the natural frequency to increase.

As previously mentioned, the mass sensing with a SWCNT-based mass sensor is based on the fact that the added mass causes a shift to the resonant frequency of the resonator. It means that the resonant frequency is sensitive to changes in the attached mass. To gain a better understanding of this fact and to explore the net effect of the attached mass on the resonant frequency of the mass sensor, the shift of frequency parameter SF is investigated for different parameters such as Pasternak-type foundation constants (k_w, k_p), aspect ratio L/d_o, nonlocal parameter e_0a and the position of nanomass X_m/L. Moreover, according to equation (20), increasing the SF parameter indicates that the mass sensitivity is increased.

Figures 5–9 show the shift of frequency SF as a function of the mass ratio MR, while the impacts of a single specific parameter have been studied in each figure. It can be seen from all these figures that SF increases with increasing the MR. Therefore, a high-mass sensitivity is revealed for nanoparticles with high masses. It should be noted that for a nanoparticle with very large mass (more than 10^4 times greater than the mass of the carbon nucleus), the nanotube does not need to be sensed because these masses are larger than the mass of the nanotube.

As mentioned above, the natural frequency is sensitive to the stiffness of the boundaries. Therefore, the effects of three typical boundary conditions on the SF parameter

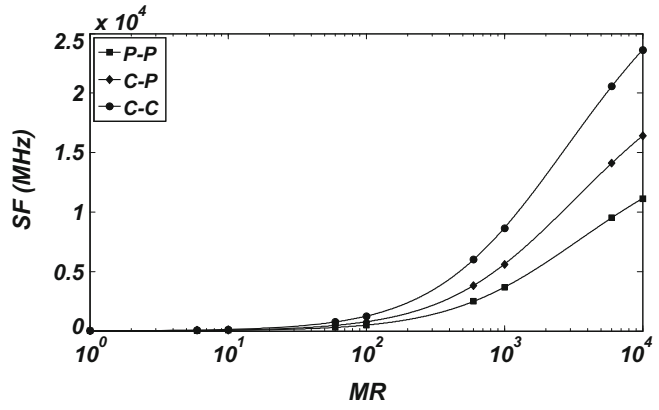

Fig. 5. The shift of frequency SF against the mass ratio MR for three standard boundary conditions.

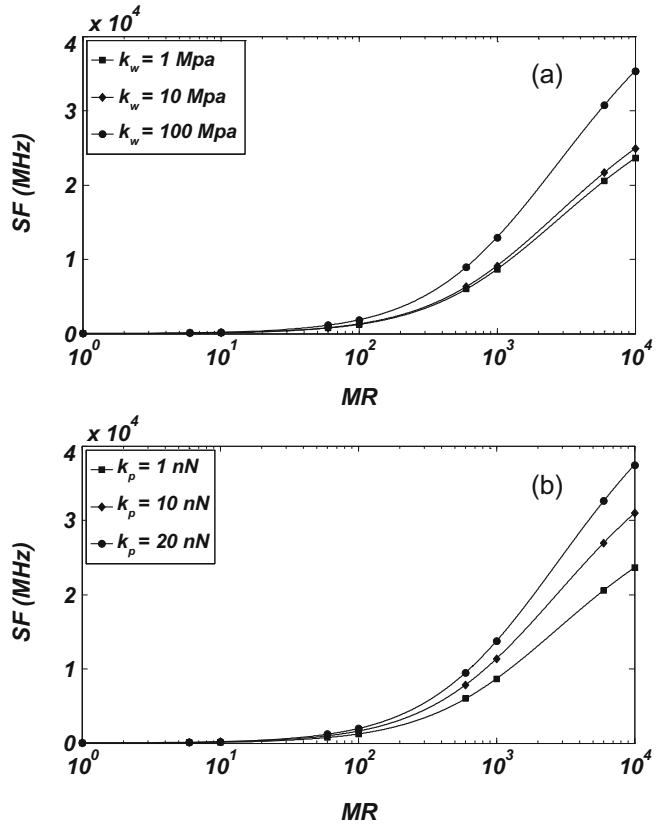

Fig. 6. The shift of frequency SF against the mass ratio MR for different values of (a) the Winkler stiffness k_w and (b) the shearing layer stiffness k_p.

are shown in Figure 5. This figure depicts that the SF for C-C boundary condition has higher values than other boundary conditions, due to the increased stiffness of the model. Hence, for the remaining parts of the paper, the SF is calculated for SWCNT with C-C boundary condition with an attached mass.

Figure 6 shows the influence of the surrounding elastic medium on the SF versus the MR. The results demonstrate that with increasing stiffness of the medium, due to increasing the Winkler stiffness k_w and/or the shearing

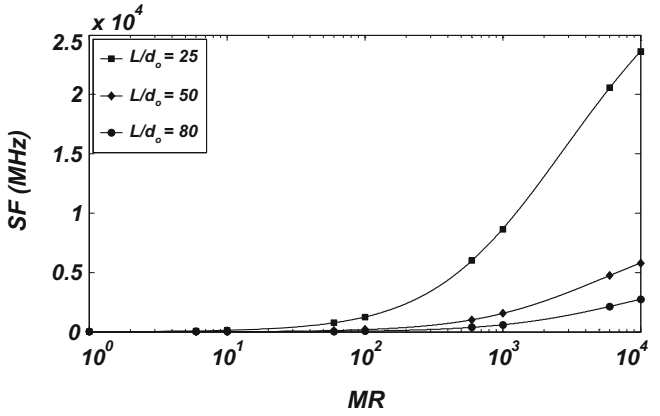

Fig. 7. The shift of frequency SF against the mass ratio MR for different values of the aspect ratio L/d_o.

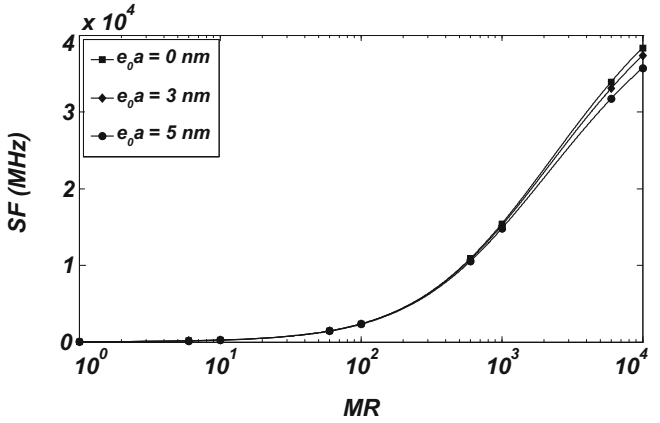

Fig. 8. The shift of frequency SF against the mass ratio MR for different values of the nonlocal parameter e_0a.

layer stiffness k_p, the amount of the shift of frequency increases significantly. This indicates that as the nanotube vibrates in a stiffer medium, the total stiffness of the system K_{eq} is increased and higher mass sensitivity followed.

The SF parameter is highly sensitive to the dimensions of the SWCNT. Therefore, Figure 7 examines the effect of the aspect ratio L/d_o on the shift of frequency SF against the mass ratio MR. It is clear from the figure that for long and slender SWCNTs with a high aspect ratio L/d_o, the SF declines, and the effects of an attached mass on the rise of frequency reduce. With reducing the aspect ratio in short SWCNTs, the total stiffness K_{eq} remains constant while the total mass of the system M_{eq} decreases. This can explain why the mass sensitivity increases in stocky nanotubes.

Figure 8 illustrates the importance of the nonlocal elasticity and nanoscale effects in determining the SF. The nonlocal elasticity theory results in a prediction that the SWCNT becomes more flexible and reduces the stiffness of this structure. Therefore, with an increase in SWCNT stiffness by a decrease in the nonlocal parameter e_0a, the SF increases consequently. It can be seen that the larger shift of frequency occurred at the lower values of the nonlocal parameter.

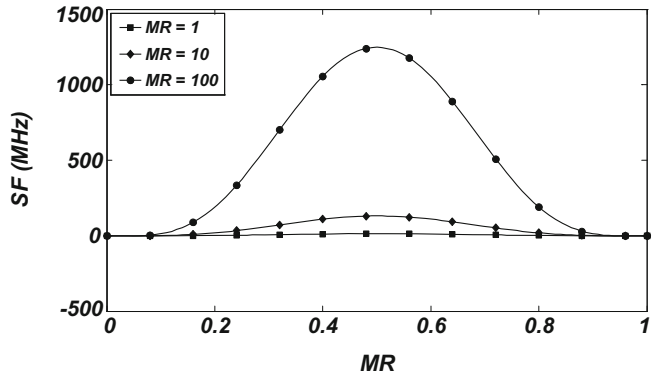

Fig. 9. The shift of frequency SF against the location of the attached mass X_m/L for different values of the mass ratio MR.

Finally, the position of any added mass can be important for the frequency shift of the mass sensor. Figure 9 illustrates the relationship between shift of frequency SF and location of attached mass X_m. The SF is plotted as a function of X_m/L with different values of the mass ratio (MR = 1, 10, 100). It can be found that the shift of frequency increases when the position of attached mass is converging to an intermediate location of C-C SWCNT especially in $MR = 100$, because the maximum displacement occurs at this point for this kind of boundary condition.

5 Conclusion and future outlook

CNTs have many applications in biological technology [13–15], especially in medical applications [16], and sensors [6,7]. Therefore, in this study, based on the nonlocal Euler-Bernoulli theory, the dynamic behavior of an embedded SWCNT carrying a nanoparticle has been performed, as a mass sensor. The obtained governing equation of motion is solved by the Galerkin method, and the fundamental frequency is calculated. The results from the nonlocal continuum-based elasticity model agree well with numerical data of MD simulation published in the literature, while the local ones in a previous study show a significant deviation. The results indicate that the resonant frequencies decrease by an increase in the mass of the nanoparticle and decreasing the stiffness of SWCNTs. The shift of frequency due to a change in the value of attached mass illustrates the sensitivity of the SWCNT-based mass sensor and is characterized as a sensitivity parameter. Detailed results demonstrated that the sensor sensitivity rises by increasing the mass ratio, especially for stocky SWCNT, with stiff foundation, the small values of the nonlocal coefficient and for high boundary stiffness. Furthermore, by moving the added mass from the boundaries of SWCNT to the center, the shift of frequency increases.

Appendix

The parameters $K_{\rm eq}$ and $M_{\rm eq}$ for different boundary conditions:
P-P conditions:

$$K_{\rm eq} = \left(-\frac{e_0a^2\pi^4}{2L^3} - \frac{\pi^2}{2L}\right)k_p + \left(-\frac{e_0a^2\pi^2}{2L} - \frac{L}{2}\right)k_w - \frac{EI\pi^4}{2L^3}$$

$$M_{\rm eq} = \rho A\left(-\frac{e_0a^2\pi^2}{2L} - \frac{L}{2}\right) + m\left(\sin\left(\frac{\pi X_m}{L}\right)^2 \text{Heaviside}(X_m - L) - \frac{\sin\left(\frac{\pi X_m}{L}\right)^2 e_0a^2\pi^2\text{Heaviside}(X_m)}{L^2} - \frac{\sin\left(\frac{\pi X_m}{L}\right)^2 e_0a^2\pi^2\text{Heaviside}(X_m)}{L^2} - \sin\left(\frac{\pi X_m}{L}\right)^2 \text{Heaviside}(X_m)\right).$$

C-P conditions:

$$K_{\rm eq} = \left(-\frac{223e_0a^2}{L^3} - \frac{11.6}{L}\right)k_p + \left(-\frac{11.6e_0a^2}{L} - 0.9L\right)k_w - \frac{223EI}{L^3}$$

$$\begin{aligned} M_{\rm eq} = {} & \rho A\left(-\frac{11.6e_0a^2}{L} - 0.9L\right) + m\left(-2\cosh\left(\frac{3.92X_m}{L}\right) \times \text{Heaviside}(X_m)\sin\left(\frac{3.92X_m}{L}\right)\right. \\ & - 2\sinh\left(\frac{3.92X_m}{L}\right)\text{Heaviside}(X_m - L)\sin\left(\frac{3.92X_m}{L}\right) + 2\cosh\left(\frac{3.92X_m}{L}\right)\text{Heaviside}(X_m)\sinh\left(\frac{3.92X_m}{L}\right) \\ & + 2\cosh\left(\frac{3.92X_m}{L}\right)\text{Heaviside}(X_m)\cos\left(\frac{3.92X_m}{L}\right) + 2\cosh\left(\frac{3.92X_m}{L}\right)\text{Heaviside}(X_m - L)\sin\left(\frac{3.92X_m}{L}\right) \\ & - 2\cosh\left(\frac{3.92X_m}{L}\right)\text{Heaviside}(X_m - L)\cos\left(\frac{3.92X_m}{L}\right) + 2\cosh\left(\frac{3.92X_m}{L}\right)\text{Heaviside}(X_m - L)\sinh\left(\frac{3.92X_m}{L}\right) \\ & \left. - 2\sinh\left(\frac{3.92X_m}{L}\right)\text{Heaviside}(X_m)\cos\left(\frac{3.92X_m}{L}\right) + 2\sinh\left(\frac{3.92X_m}{L}\right)\text{Heaviside}(X_m)\cos\left(\frac{3.92X_m}{L}\right)\right) \end{aligned}$$

$$
\begin{aligned}
&- 2\sin\left(\frac{3.92X_m}{L}\right)\text{Heaviside}(X_m - L)\cos\left(\frac{3.92X_m}{L}\right) + 2\sinh\left(\frac{3.92X_m}{L}\right)\text{Heaviside}(X_m)\sin\left(\frac{3.92X_m}{L}\right)\\
&+ 2\sinh\left(\frac{3.92X_m}{L}\right)\text{Heaviside}(X_m - L)\cos\left(\frac{3.92X_m}{L}\right) - \frac{1}{L^2}\left(15.4\cosh\left(\frac{3.92X_m}{L}\right)^2 e_0a^2\text{Heaviside}(X_m - L)\right)\\
&+ \frac{1}{L^2}\left(15.4\cosh\left(\frac{3.92X_m}{L}\right)^2 e_0a^2\text{Heaviside}(X_m)\right) - \frac{1}{L^2}\left(15.6\sinh\left(\frac{3.92X_m}{L}\right)^2 e_0a^2\text{Heaviside}(X_m - L)\right)\\
&+ \frac{1}{L^2}\left(15.6\sinh\left(\frac{3.92X_m}{L}\right)^2 e_0a^2\text{Heaviside}(X_m)\right) + \frac{1}{L^2}\left(15.4\cos\left(\frac{3.92X_m}{L}\right)^2 e_0a^2\text{Heaviside}(X_m - L)\right)\\
&- \frac{1}{L^2}\left(15.4\cos\left(\frac{3.92X_m}{L}\right)^2 e_0a^2\text{Heaviside}(X_m)\right) + \frac{1}{L^2}\left(15.6\sin\left(\frac{3.92X_m}{L}\right)^2 e_0a^2\text{Heaviside}(X_m - L)\right)\\
&- \frac{1}{L^2}\left(15.6\sin\left(\frac{3.92X_m}{L}\right)^2 e_0a^2\text{Heaviside}(X_m)\right) + \left(\frac{31\cosh\left(\frac{3.92X_m}{L}\right)\text{Heaviside}(X_m - L)\sinh\left(\frac{3.92X_m}{L}\right)e_0a^2}{L^2}\right)\\
&- \left(\frac{31\cosh\left(\frac{3.92X_m}{L}\right)\text{Heaviside}(X_m)\sinh\left(\frac{3.92X_m}{L}\right)e_0a^2}{L^2}\right)\\
&- \left(\frac{31\cos\left(\frac{3.92X_m}{L}\right)\text{Heaviside}(X_m - L)\sin\left(\frac{3.92X_m}{L}\right)e_0a^2}{L^2}\right)\\
&+ \left(\frac{31\cos\left(\frac{3.92X_m}{L}\right)\text{Heaviside}(X_m)\sin\left(\frac{3.92X_m}{L}\right)e_0a^2}{L^2}\right) + \sin\left(\frac{3.92X_m}{L}\right)^2\text{Heaviside}(X_m - L)\\
&- \sin\left(\frac{3.92X_m}{L}\right)^2\text{Heaviside}(X_m) + \sinh\left(\frac{3.92X_m}{L}\right)^2\text{Heaviside}(X_m - L)\\
&+ \cosh\left(\frac{3.92X_m}{L}\right)^2\text{Heaviside}(X_m - L) + \cos\left(\frac{3.92X_m}{L}\right)^2\text{Heaviside}(X_m - L)\\
&- \cosh\left(\frac{3.92X_m}{L}\right)^2\text{Heaviside}(X_m) - \cos\left(\frac{3.92X_m}{L}\right)^2\text{Heaviside}(X_m) - \sinh\left(\frac{3.92X_m}{L}\right)^2\text{Heaviside}(X_m)\Bigg).
\end{aligned}
$$

C-C conditions:

$$
\begin{aligned}
K_{\text{eq}} &= \left(-\frac{500.5e_0a^2}{L^3} - \frac{12.3}{L}\right)k_p + \left(-\frac{12.3e_0a^2}{L} - L\right)k_w - \frac{500.5EI}{L^3}\\
M_{\text{eq}} &= \rho A\left(-\frac{11.6e_0a^2}{L} - 0.9L\right) + m\left(1.96\cosh\left(\frac{4.73X_m}{L}\right)\text{Heaviside}(X_m - L)\sinh\left(\frac{4.73X_m}{L}\right)\right.\\
&- 1.96\cosh\left(\frac{4.73X_m}{L}\right)\text{Heaviside}(X_m)\sin\left(\frac{4.73X_m}{L}\right) - 1.96\cos\left(\frac{4.73X_m}{L}\right)\text{Heaviside}(X_m)\sinh\left(\frac{4.73X_m}{L}\right)\\
&+ 1.93\cos\left(\frac{4.73X_m}{L}\right)\text{Heaviside}(X_m)\sinh\left(\frac{4.73X_m}{L}\right) + 1.96\cosh\left(\frac{4.73X_m}{L}\right)\text{Heaviside}(X_m)\sinh\left(\frac{4.73X_m}{L}\right)\\
&+ 1.96\cos\left(\frac{4.73X_m}{L}\right)\text{Heaviside}(X_m)\sin\left(\frac{4.73X_m}{L}\right) - 1.96\cos\left(\frac{4.73X_m}{L}\right)\text{Heaviside}(X_m - L)\sin\left(\frac{4.73X_m}{L}\right)\\
&+ 2\cosh\left(\frac{4.73X_m}{L}\right)\text{Heaviside}(X_m)\cos\left(\frac{4.73X_m}{L}\right) - 1.96\sinh\left(\frac{3.92X_m}{L}\right)\text{Heaviside}(X_m - L)\cosh\left(\frac{3.92X_m}{L}\right)\\
&- 1.93\sin\left(\frac{4.73X_m}{L}\right)\text{Heaviside}(X_m - L)\sinh\left(\frac{4.73X_m}{L}\right) + 1.96\cosh\left(\frac{4.73X_m}{L}\right)\text{Heaviside}(X_m - L)\sin\left(\frac{4.73X_m}{L}\right)\\
&- 2\cosh\left(\frac{4.73X_m}{L}\right)\text{Heaviside}(X_m - L)\cos\left(\frac{4.73X_m}{L}\right) + \frac{1}{L^2}\left(22.3\cos\left(\frac{4.73X_m}{L}\right)^2 e_0a^2\text{Heaviside}(X_m - L)\right)
\end{aligned}
$$

$$
\begin{aligned}
&-\frac{1}{L^2}\left(22.3\cosh\left(\frac{4.73X_m}{L}\right)^2 e_0a^2\text{Heaviside}(X_m-L)\right)+\frac{1}{L^2}\left(22.3\cosh\left(\frac{4.73X_m}{L}\right)^2 e_0a^2\text{Heaviside}(X_m)\right)\\
&-\frac{1}{L^2}\left(22.3\cos\left(\frac{4.73X_m}{L}\right)^2 e_0a^2\text{Heaviside}(X_m)\right)-\frac{1}{L^2}\left(21.5\sinh\left(\frac{4.73X_m}{L}\right)^2 e_0a^2\text{Heaviside}(X_m-L)\right)\\
&+\frac{1}{L^2}\left(21.5\sinh\left(\frac{4.73X_m}{L}\right)^2 e_0a^2\text{Heaviside}(X_m)\right)+\frac{1}{L^2}\left(21.5\sin\left(\frac{4.73X_m}{L}\right)^2 e_0a^2\text{Heaviside}(X_m-L)\right)\\
&-\frac{1}{L^2}\left(21.5\sin\left(\frac{4.73X_m}{L}\right)^2 e_0a^2\text{Heaviside}(X_m)\right)+\left(\frac{43.9\cosh\left(\frac{4.73X_m}{L}\right)\text{Heaviside}(X_m-L)\sinh\left(\frac{4.73X_m}{L}\right)e_0a^2}{L^2}\right)\\
&-\left(\frac{43.9\cosh\left(\frac{4.73X_m}{L}\right)\text{Heaviside}(X_m)\sinh\left(\frac{4.73X_m}{L}\right)e_0a^2}{L^2}\right)\\
&-\left(\frac{43.9\cos\left(\frac{4.73X_m}{L}\right)\text{Heaviside}(X_m-L)\sin\left(\frac{4.73X_m}{L}\right)e_0a^2}{L^2}\right)\\
&+\left(\frac{43.9\cos\left(\frac{4.73X_m}{L}\right)\text{Heaviside}(X_m)\sin\left(\frac{4.73X_m}{L}\right)e_0a^2}{L^2}\right)\\
&+\cos\left(\frac{4.73X_m}{L}\right)^2\text{Heaviside}(X_m-L)-\sin\left(\frac{4.73X_m}{L}\right)^2\text{Heaviside}(X_m)\\
&+0.96\sinh\left(\frac{4.73X_m}{L}\right)^2\text{Heaviside}(X_m-L)+0.96\sin\left(\frac{4.73X_m}{L}\right)^2\text{Heaviside}(X_m-L)\\
&-\cosh\left(\frac{4.73X_m}{L}\right)^2\text{Heaviside}(X_m)-0.96\sinh\left(\frac{4.73X_m}{L}\right)^2\text{Heaviside}(X_m)\\
&-\cos\left(\frac{4.73X_m}{L}\right)^2\text{Heaviside}(X_m)+\cosh\left(\frac{4.73X_m}{L}\right)^2\text{Heaviside}(X_m-L)\Bigg).
\end{aligned}
$$

References

1. G. Che, B.B. Lakshmi, E.R. Fisher, C.R. Martin, Nature **393**, 346 (1998)
2. T. Ebbesen, *Carbon Nanotubes: Preparation and Properties* (CRC Press, New York, 1997)
3. S.-C. Fang, W.-J. Chang, Y.-H. Wang, Phys. Lett. A **371**, 499 (2007)
4. A. Garg, S.B. Sinnott, Chem. Phys. Lett. **295**, 273 (1998)
5. E.T. Thostenson, Z. Ren, T.-W. Chou, Chem. Phys. Lett. **61**, 1899 (2001)
6. L. Gu, T. Elkin, X. Jiang, H. Li, Y. Lin, L. Qu, T.-R.J. Tzeng, R. Joseph, Y.-P. Sun, Chem. Commun. **7**, 874 (2005)
7. Y. Lin, S. Taylor, H. Li, K.A.S. Fernando, L. Qu, W. Wang, L. Gu, B. Zhou, Y.-P. Sun, J. Mater. Chem. **14**, 527 (2004)
8. C. Li, T.-W. Chou, Phys. Rev. B **68**, 073405 (2003)
9. R.H. Baughman, C. Cui, A.A. Zakhidov, Z. Iqbal, J.N. Barisci, G.M. Spinks, G.G. Wallace, A. Mazzoldi, D. De Rossi, A.G. Rinzler, O. Jaschinski, S. Roth, M. Kertesz, Science **284**, 1340 (1999)
10. L. Lacerda, S. Raffa, M. Prato, A. Bianco, K. Kostarelos, Nano Today **2**, 38 (2007)
11. M. Prato, K. Kostarelos, A. Bianco, Acc. Chem. Res. **41**, 60 (2007)
12. U. Yogeswaran, S.-M. Chen, Sensors **8**, 290 (2008)
13. J.J. Davis, M.L.H. Green, H. Allen, O. Hill, Y.C. Leung, P.J. Sadler, J. Sloan, A.V. Xavier, S. Chi Tsang, Inorg. Chem. Acta **272**, 261 (1998)
14. M. Mattson, R. Haddon, A. Rao, J. Mol. Neurosci. **14**, 175 (2000)
15. S.C. Tsang, J.J. Davis, M.L.H. Green, H.A.O. Hill, Y.C. Leung, P.J. Sadler, J. Chem. Soc. Chem. Commun. **272**, 1803 (1995)
16. F. Lu, L. Gu, M.J. Meziani, X. Wang, P.G. Luo, L.M. Veca, L. Cao, Y.-P. Sun, Adv. Mat. **21**, 139 (2009)
17. S.S. Wong, E. Joselevich, A.T. Woolley, C.L. Cheung, C.M. Lieber, Nature **394**, 52 (1998)
18. R. Chowdhury, S. Adhikari, J. Mitchell, Phys. E: Low-Dimens. Syst. Nanostruct. **42**, 104 (2009)
19. K. Jensen, K. Kim, A. Zettl, Nature Nanotechnol. **3**, 533 (2008)
20. T. Murmu, S.C. Pradhan, Phys. E: Low-Dimens. Syst. Nanostruct. **41**, 1232 (2009)
21. L. Wang, Q. Ni, Comput. Mater. Sci. **43**, 399 (2008)
22. Z. Dendzik, M. Kosmider, M. Skrzypek, Z. Gburski, J. Mol. Struct. **704**, 203 (2004)
23. J. Won Kang, K.-S. Kim, K. Ryang Byun, E.-S. Kang, J. Lee, O. Kuen Kwon, Y. Gyu Choi, H.J. Hwang, Phys. E: Low-Dimens. Syst. Nanostruct. **42**, 1995 (2010)

24. S.K. Georgantzinos, N.K. Anifantis, Phys. E: Low-Dimens. Syst. Nanostruct. **42**, 1795 (2010)
25. B. Arash, Q. Wang, V.K. Varadan, J. Nanotechnol. Eng. Med. **2**, 021010 (2011)
26. A.Y. Joshi, S.P. Harsha, S.C. Sharma, Phys. E: Low-Dimens. Syst. Nanostruct. **42**, 2115 (2010)
27. I. Mehdipour, A. Barari, G. Domairry, Comput. Mater. Sci. **50**, 1830 (2011)
28. T. Murmu, S. Adhikari, Mech. Res. Commun. **38**, 62 (2011)
29. T. Murmu, S. Adhikari, Sens. Actuators A Phys. (2011)
30. M. Aydogdu, S. Filiz, Phys. E: Low-Dimens. Syst. Nanostruct. **43**, (2011)
31. M. Simsek, Phys. E: Low-Dimens. Syst. Nanostruct. **43**, 182 (2010)
32. A.C. Eringen, J. Appl. Phys. **54**, 4703 (1983)
33. S. Rao, *Vibration of Continuous Systems* (Wiley, Hoboken, New Jersey, 2007)
34. S.S. Gupta, F.G. Bosco, R.C. Batra, Comput. Mater. Sci. **47**, 1049 (2010)